TÜBİTAK

Turkish Journal of Electrical Engineering & Computer Sciences

http://journals.tubitak.gov.tr/elektrik/

Research Article

Turk J Elec Eng & Comp Sci
(2015) 23: 17 – 27

doi:10.3906/elk-1204-44

Simulation of locating buried objects via fringe pattern-based measurements in an optical fiber sensor-integrated continuous-wave ground-penetrating radar system

Asaf Behzat ŞAHİN*, **Hatice Gonca BULUR**
Yıldırım Beyazıt University, Ulus, Ankara, Turkey

Received: 16.04.2012 • **Accepted:** 12.11.2012 • **Published Online:** 12.01.2015 • **Printed:** 09.02.2015

Abstract: A new ground-penetrating radar system that can determine the depth and position of a buried metal cylinder, which is the combination of an optical fiber sensor (OFS), continuous-wave transmitter, and optical communication link, is proposed and simulated in the MATLAB and Optiwave program packages. Employing an optical sensor instead of a standard radio frequency (RF) receiver offers the advantage of preventing electromagnetic interference along the sensor's main unit cable and lower amplification noise. In this paper, the electric field distribution at the OFS due to reflections from the soil surface and the buried object is obtained mathematically using Green's function. The OFS's detected electric signal is then simulated. The effects of the cylinder's depth and the RF transmitter frequency are observed. The plots of the OFS output voltages vs. the x-axis distance to the burial point display interference fringe patterns. The position and the depth of the cylinder are determined using the characteristics of these patterns. It is estimated that the burial depth can be ascertained with a maximum 5-cm error for a 1-GHz transmitter frequency.

Key words: Detection, ground-penetrating radar, optical fiber sensor, interference fringe pattern, electric field distribution

1. Introduction

Ground-penetrating radar (GPR) is an electromagnetic (EM) geophysical technique that is used for detecting, imaging, and mapping below a surface [1]. A typical GPR system consists of a transmitting and a receiving antenna. When an EM wave is sent from a transmitting antenna into the subsurface, it is scattered and reflected whenever it faces any discontinuity. Those reflections are then measured and collected by the receiving antenna.

The first GPR implementation was demonstrated by Hülsmeyer in 1904, and the related techniques were developed as early as the 1930s [2]. However, the basic principles of optical fiber sensors (OFSs) have been known for more than 40 years and technological studies in this field have been steadily increasing since the 1990s [3]. Although there are many studies related to only GPR or OFS, there are not many studies involving both. Previously, some experiments were performed to estimate the direction of the waves using borehole radar [4]. The borehole radar, which consists of an OFS array, is used in places where GPR cannot reach. The multiple signal classification algorithm is applied to estimate the source position by a borehole.

There are several studies on detecting landmines using bistatic-type GPR systems [5–7]. These systems consist of a transverse EM horn antenna as a transmitter and a passive optical sensor as a receiver. A network analyzer is used as a receiver or a transmitter. The sensor scans the surface using a positioner and synthetic aperture processing is applied to obtain the image of the buried object. The sensor is tested in both stepped

*Correspondence: absahin@ybu.edu.tr

frequency and impulse radar systems. The data are acquired by both stepped and continuous data modes. A time domain data acquisition system may be employed instead of a vector network analyzer; the data are preprocessed by pulse compression, image reconstruction is performed by diffraction stacking, and an F-k filtering algorithm is developed to suppress the effect of the strong incoming signals [8,9].

Array-type directional borehole radar systems may detect the target's azimuth location [10]. The system consists of a dipole antenna as a transmitter and optical electric field sensors as a receiver. The phase differences among the sensors are determined to obtain the azimuth angle of the target and to observe the effects of mutual coupling. An Adcock direction-finding algorithm is developed to increase the azimuth sensitivity and to obtain the 3-dimensional (3D) images of the targets [11,12]. The cross-hole and single-hole configurations are performed to detect the azimuth direction. The RAMAC directional borehole radar system is an alternative way to obtain the same results. The target's azimuth orientations may also be inferred by array-type directional borehole radar systems [13,14]. The system consists of a dipole antenna as a transmitter and optical electric field sensors as a receiver. The azimuth orientations are obtained by combining the in situ calibration technique with single-hole measurement configuration. The in situ calibration technique, which equalizes the sensitivity of each receiver, is developed due to differences in sensitivity.

In this paper, a different optical GPR system is studied and its utility in locating buried objects is simulated [15]. It consists of a continuous-wave radio frequency (RF) transmitter, a target (circular cylinder), and an OFS interrogation system (OFSIS). The OFSIS consists of a light source (laser as a transmitter), an OFS, and a photodetector (PD) (as a receiver) (Figure 1) Medium 1 is air OFS and medium 2 is dry soil. The circular cylinder, which has a radius of 5 cm, is completely buried in the dry soil. The transmitter is placed 100 m above the surface for plane wave arrival assumption, with a 1-W/cm^2 power intensity at the surface. The operating frequency of the system is varied between 100 MHz and 1 GHz. The purpose of this system is to detect the buried cylinder's depth and position.

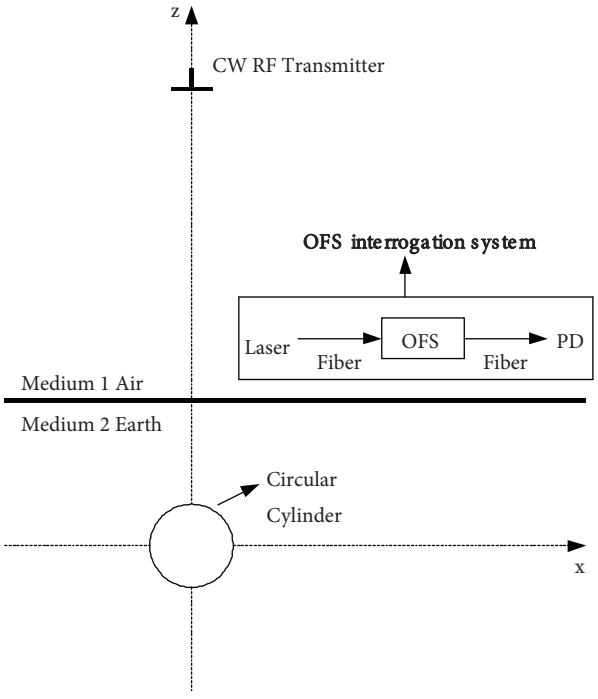

Figure 1. The configuration of the GPR system.

When compared to previous ones, in this study, the GPR is used instead of borehole radar. The configurations of the systems are similar, but their working methods are different. The system does not require a vector network analyzer and none of the acquisition modes are tested. Instead of the azimuth angle and direction, the depth and position of the target are determined. The receiver consists of a short dipole and it moves along the x axis to obtain the voltage measurements inside the electric field distribution. Although the system is not set up in a laboratory environment, the MATLAB code for the OFS is coded in order to simulate the measurement of the voltages induced on the OFS. The OFS output voltage values are employed in determining the depth and position of the cylinder via the MATLAB and Optiwave programs.

2. OFS-integrated GPR system

The configuration of the GPR system is shown in Figure 1. The OFS consists of an optical modulator (Mach–Zehnder modulator) and an electric field probe, and there are no active electrical components, amplifiers, or RF cables on the OFS. The OFS modulates the optical signal amplitude according to the electric field. The constant power output of a laser light source, 1-mW power and 1550-nm wavelength, is fiber-connected to the optical waveguides that are embedded in a lithium niobate board. The electric field coupled to the 5-cm-long electric field probe antenna affects the optical wave propagating through the waveguides. The optical phase shift variation between 2 optical paths is induced by an electro-optic effect. As a result, interference occurs at the output and the optical intensity changes. The modulated light is fiber-coupled, received at the PD at the end of the sensor fiber line, converted into an electric current at a PIN photodiode, and the output is transamplified as a sensor output voltage (Vread) signal. The main advantage of this configuration is that the field measurement and sensor supply/readout parts are optically isolated from each other; hence, the transmission line noise inherent to the RF cable systems is reduced considerably [16]. The configuration of the OFS is shown in Figure 2.

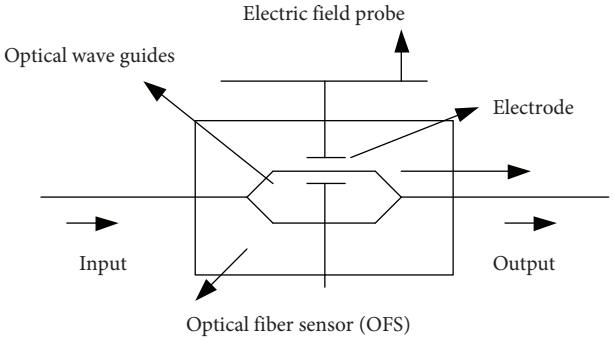

Figure 2. The configuration of the OFS.

The circular cylinder of radius a is deeply buried inside of the dielectric half-space, and a is assumed to be 5 cm. The depth from the interface to the center of the cylinder is b. The cylinder is placed at the origin, and the transmitter is assumed to be far above the interface for parallel wave approximation, so that a continuous plane wave with a 1-W/cm^2 power concentration arrives perpendicular to the soil surface. The Debye model is used to characterize the dielectric properties of soils [17]. The parameters of a sample of martian soil is used in the study and it is very dry [18]. Air and soil permeabilities and air permittivity are unitary. The permittivity of dry soil obtained from this model is equal to 3.56 and the attenuation is small.

2.1. Electric field strength at the OFS

The electric field strength that is observed by the OFS is obtained analytically [19]. The electric field strength is equal to the total scattered electric field above the interface, which is equal to the summation of the reflected electric field from the surface and the electric field scattered from the buried cylinder. It is obtained as:

$$Etotal = \frac{(n-1)}{(n+1)} \exp\{-ik_1(z-b)\} + \frac{-8k_1^2}{\sqrt{2\pi}(k_1^2-k_2^2)(k_1+k_2)} \exp\left(ik_2 b - ik_1 b \sin\varphi + ib\sqrt{k_2^2 - k_1^2\cos^2\varphi}\right)$$
$$\times \left\{k_1 \sin^2\varphi - \sin\varphi\sqrt{k_2^2 - k_1^2\cos^2\varphi}\right\} \sum_{n=-\infty}^{n=\infty} \left\{\frac{(i)^n J_n(k_2 a)\exp(in\varphi_o)}{H_n^{(1)}(k_2 a)}\right\} \times \frac{\exp(ik_i\rho - i^{\pi}/4)}{\sqrt{k_1\rho}} \quad (1)$$

where k_1 is the propagation constant of medium 1, k_2 is the propagation constant of medium 2, J_n is the Bessel function, $H_n^{(1)}$ is the first-order Hankel function, n is the index of refraction, and φ is the angle of incidence.

2.2. Simulation method

A MATLAB analysis of the electric field distribution is performed. The total scattered electric field is coded according to Eq. (1), in order to observe the electric field distribution or strength. The operating frequency of the system is varied from 100 MHz to 1 GHz. The radius of the cylinder, a, is assumed as a 5 cm constant. The value of the depth of the cylinder, b, varies from 10 cm to 100 cm. Different distributions are observed via either changing the depth of the object or the frequency of the system. An example of the electric field distribution variation due to the height vs. the vertical displacement values is shown in Figure 3 for f = 1 GHz and b = 50 cm.

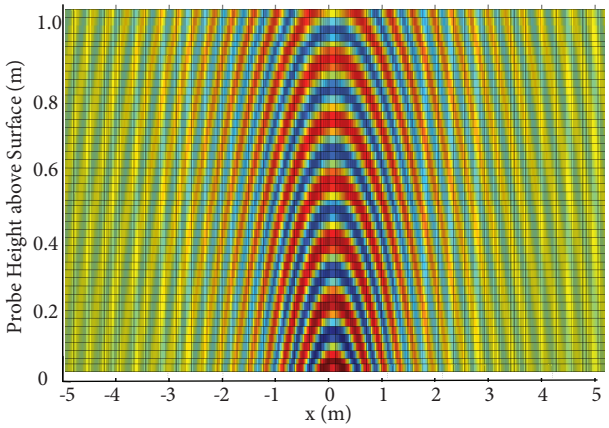

Figure 3. An example of the electric field distribution above the surface.

After the derivation of the total electric field strength propagating through the OFS, the voltages induced on the receiver antenna due to the electric field distribution are collected and measured by the sensor. The algorithm is coded with respect to the following principle: the OFS travels along the x-axis in order to measure the voltage induced due to the electric field strength variations. The x-axis interval is between –5 m and 5 m and the z-axis is between 0.1 m and 1 m, and the electric field probe length is 5 cm. The transmitter antenna induces 30 dBm/cm^2 of power density at the earth's surface and the probe is at a height of 10 cm. The frequency and impedance matching varies the electric field strength coupled to the OFS field probe antenna, and this in turn affects the Vread via the optical modulator. The generated code is executed and simulated

in the MATLAB package program. The 2D plots of the Vread vs. the x-axis displacement are obtained for different values of system frequency and the depth of the cylinder. Those plots are illustrative of interference fringe patterns, which are observed when 2 out of phase waves are superimposed.

The frequency of the system is varied from 100 MHz to 1 GHz in order to observe the Vread values at a fixed depth of b = 20 cm, radius a of 5 cm, and probe height of 10 cm. The graphs in Figure 4 display the Vread vs. the x-axis displacement for f = 500 MHz and f = 1 GHz. When the 2D plots are compared, it is seen that as the system frequency increases and the wave patterns occur more frequently, which in turn produces more wavefronts. As a result, the width of the antinode decreases, the electric field strength decreases, yet the antenna responsivity increases. Hence, there is a trade-off; at higher frequencies, there is more antenna coupling and better resolution, and at lower frequencies, the signals suffer less attenuation through the earth.

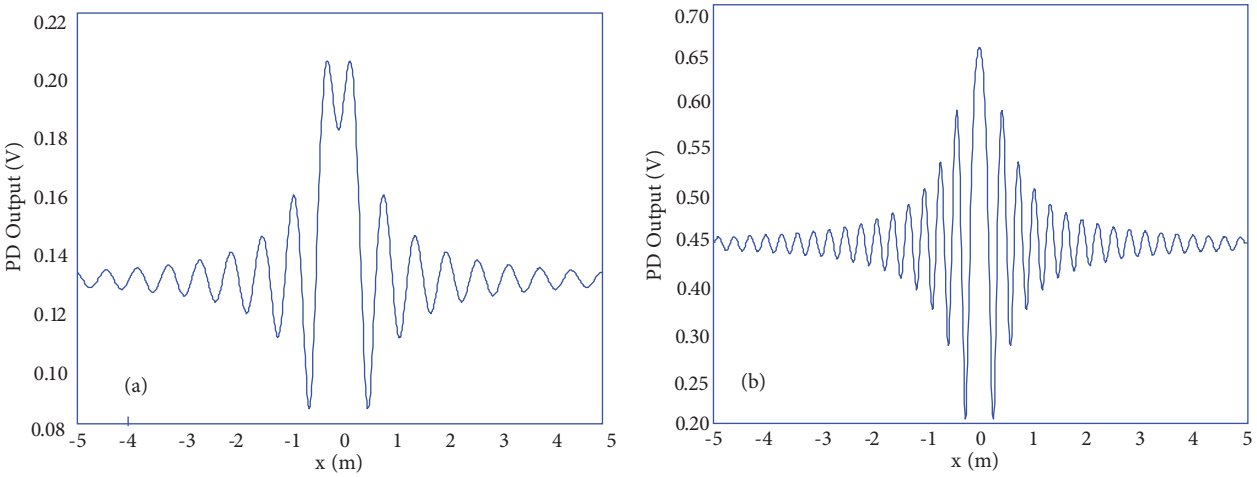

Figure 4. a) Vread vs. the x displacement for b = 20 cm, probe height = 10 cm, and f = 500 MHz; and b) Vread vs. the x displacement for b = 20 cm, probe height = 10 cm, and f = 1 GHz.

The depth of the cylinder is varied from 10 cm to 100 cm and the Vread values at a fixed frequency of f = 500 MHz are recorded for radius a at 5 cm and a probe height of 10 cm (Figure 5). When the depth of the target increases, the width of the antinode increases. Its shape goes from spherical to parabolic, to a plane wave-like appearance. Increasing the depth results in more attenuation and stronger side interference in the fringe patterns. At smaller depths, there is less attenuation and the power of the scattered wave is stronger.

In general, the radius (a) of the cylinder is constant and it is only changed to observe the Vread values at a fixed depth of b = 100 cm, frequency of f = 600 MHz, and probe height of 10 cm. The graphs in Figure 6 show the Vread vs. the x-axis displacement for different radii of a = 5 cm and a = 55 cm.

The 2D plots that are obtained in Figure 6 are compared. When the radius of the target increases, the scattering caused by the target also increases. Due to an increase in the interference, the width of the antinode decreases. As a result, the target can be detected more easily and it is possible to make more sensitive measurements.

3. Determining the cylinder's position and depth

After measuring the voltages at the electric field distribution, the cylinder's position is determined using 2D plots of the Vread vs. the x axis values. It is observed from the 2D analysis that the interference fringe patterns

are symmetric around the origin. This is where the target is buried in the soil. Symmetry can be observed from each fringe pattern and an example of how the position is obtained can be seen in Figure 7.

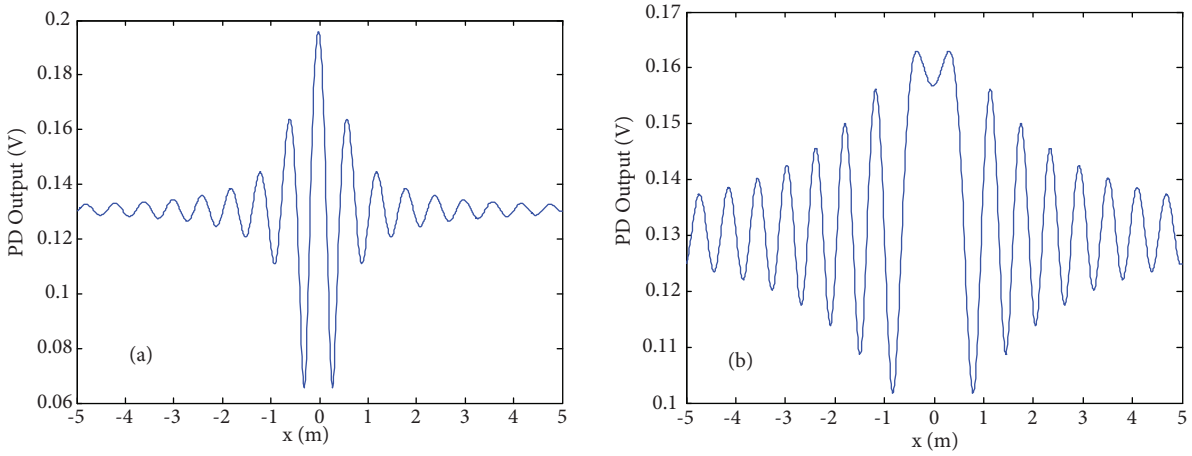

Figure 5. Sensor voltage vs. the x displacement for f = 500 MHz and probe height = 10 cm: a) depth b = 10 cm and b) depth b = 100 cm.

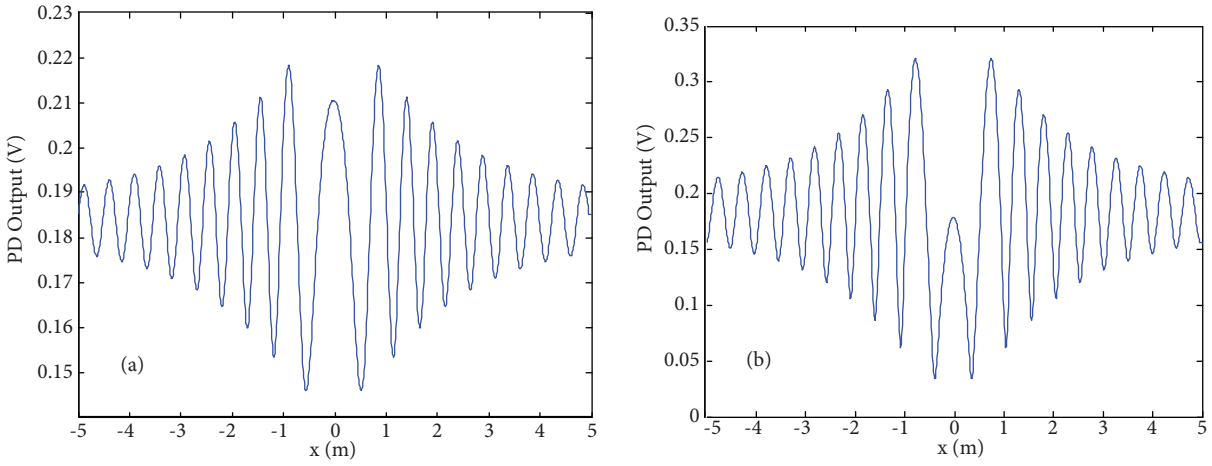

Figure 6. Vread vs. the x displacement for f = 600 MHz and depth b = 100 cm: a) radius a = 5 cm and b) radius a = 55 cm.

The cylinder's depth is also determined using the interference fringe patterns obtained previously. Interference occurs due to scatterings and it is related to the frequency, depth, and antinode. All of those are related to the interference fringe patterns. The depth of the cylinder is determined from the relative amplitude, x displacement, and depth relationships. When the interference fringe patterns are examined, it is observed that the relative amplitudes of the side interference fringe patterns increase as the depth of the cylinder increases. The relative amplitude is meant to be amplitude variations of the side interference fringe patterns oscillations. Those variations are shown in Figure 8. The envelope or the change in the relative amplitudes is shown as black lines in the figures.

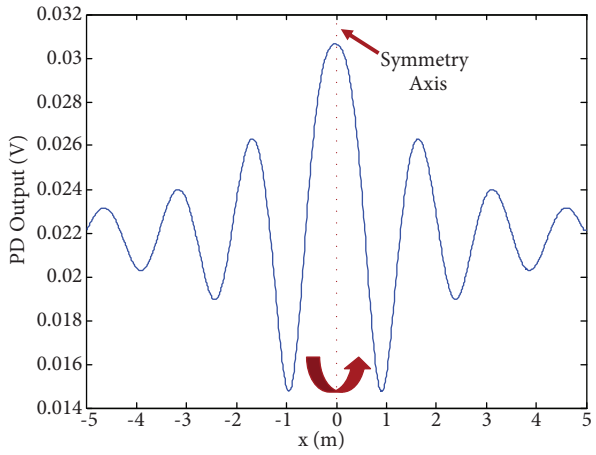

Figure 7. The inherent symmetry of interference fringe pattern.

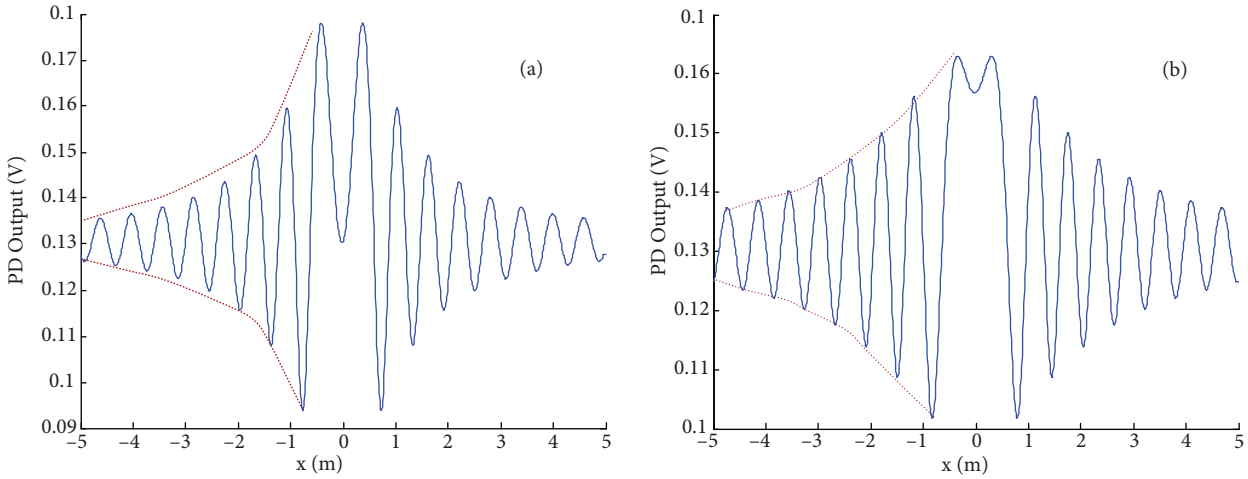

Figure 8. Interference fringe patterns for f = 500 MHz: a) depth b = 50 cm and b) depth b = 100 cm.

The relative amplitude values of the interference fringe patterns are recorded for each x displacement value by coding the MATLAB algorithm. The code analyzes each pattern. If the slope of the swing is positive, the code continues to search for the relative amplitudes. However, if the slope of the swing is negative, the code records the relative amplitude values for each x displacement value. Using the recorded values, the 2D plots of the relative amplitude vs. the x displacement (XDVRA) values are calculated for different frequency and depth trials. This process is executed and simulated in a MATLAB environment.

The 2D plots of the XDVRA values are obtained for a fixed frequency, radius (a) of 5 cm, and probe height of 10 cm. Those plots are obtained for different depths. Figure 9a shows the 2D plots for f = 1 GHz and Figure 9b shows the 2D plots for f = 500 MHz, where, as the depth of the cylinder increases, the plots' shapes approach a linear response. This is valid for all of the frequencies.

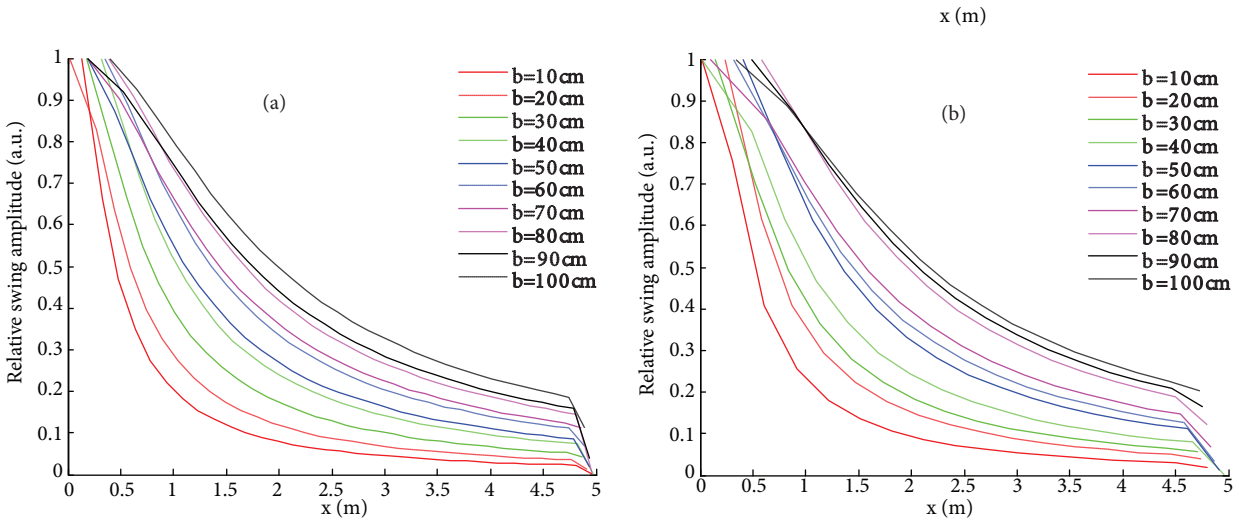

Figure 9. XDVRA values for each depth from b = 10 cm to b = 100 cm and a probe height of 10 cm, and the 2D plots for a) f = 1 GHz and b) f = 500 MHz.

The obtained 2D plots are used to measure the full-width half-maximum of the relative amplitude's distance (x displacement) to the origin (FWHMX) for each depth. Fifty percent of the amplitude is found and the related x displacement to the origin is recorded for each plot. The measurement method is demonstrated in Figure 10.

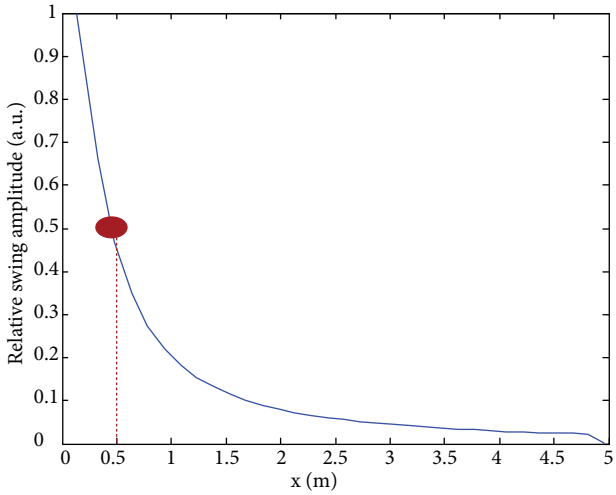

Figure 10. Full-width half-maximum measurement in the XDVRA graphs.

Since the relative amplitudes are related to the object's depth, the depth can be determined from the FWHMX. Using the recorded x displacement values, the 2D plots of the FWHMX vs. the depth are obtained. The 2D plot for f = 500 MHz is shown in Figure 11a and the same plot for f = 1 GHz is shown in Figure 11b. It is observed that, as the depth increases, the FWHMX increases. Deviation from the linear best line seems to be inversely proportional to the continuous-wave frequency, approximately 10 cm for 500 MHz and 5 cm for 1 GHz transmissions.

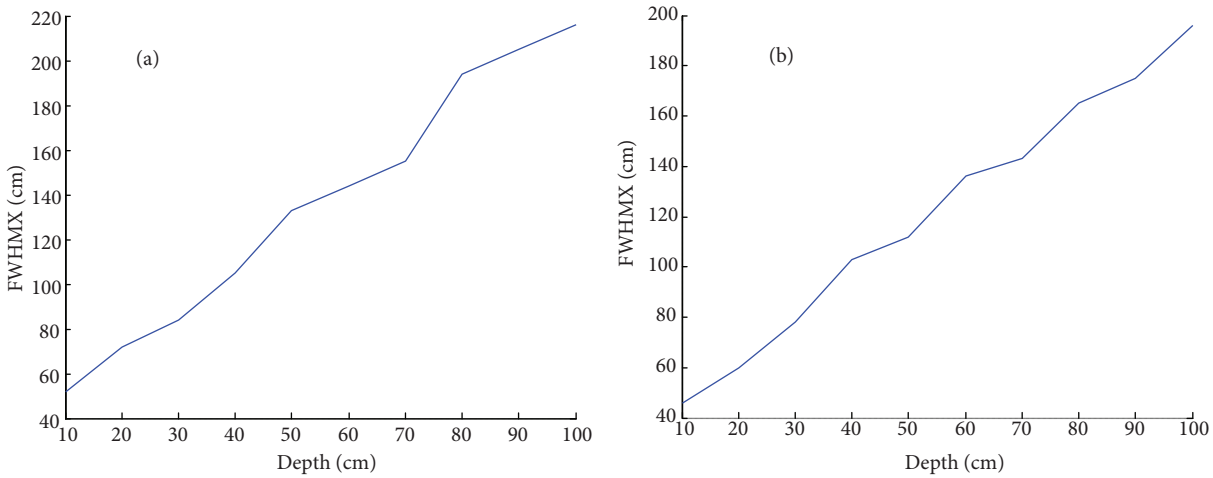

Figure 11. FWHMX vs. the buried object depth: a) f = 500 MHz and b) f = 1 GHz.

4. Conclusion

In this paper, the position and depth of a perfectly buried conducting circular cylinder can be determined by a GPR system, which consists of a transmitter, a buried object, and an OFSIS. The circular cylinder is assumed to be buried in dry soil. The Debye model is used to determine the permittivity value of the dry soil.

The electric field distribution coming through the OFS is determined mathematically by integrating Green's function over the induced current distribution. The voltages inside the distribution are then measured by the OFS and 2D plots of the Vreads vs. the x-axis displacement are obtained, which are related to the interference fringe patterns.

The position of the cylinder can be determined from the symmetry of the interference fringe patterns with a few centimeters of error. However, the depth of the cylinder is determined using the relative amplitude, x displacement, and depth relationship of the interference fringe patterns. Using this measurement method, the depth of the object can be estimated in a linear fashion. Increasing the frequency improves the sensitivity of detection. At a 1-GHz system frequency, the depth of a cylindrical object can be estimated with a 5-cm error.

As a result, in this paper, a novel GPR and OFS system integration and a new method for sensor readout interpretation are proposed. In future, laboratory and field studies will be performed in order to test the efficiency of these proposals. Moreover, numerical studies for the detection of noncircular and more irregular-shaped objects will be one of the objectives. It is expected that the shape of the object will affect the interference fringe patterns, yet in order to comment on that, additional studies and simulations will be performed in the future.

References

[1] J.M. Lopez-Higuera, Handbook of Optical Fibre Sensing Technology, New York, Wiley, 2002.

[2] D.J. Daniels, Ground Penetrating Radar, 2nd Edition, United Kingdom, The Institution of Electrical Engineers, 2004.

[3] G.C. Righini, A. Tajani, A. Cutolo, An Introduction to Optoelectronic Sensors, Singapore, World Scientific Publishing, 2009.

[4] S. Ebihara, M. Sato, "Application of an optical electric field sensor array for direction of arrival estimation in a borehole", Proceedings of the IEEE International Geoscience and Remote Sensing Symposium, Vol. 3, pp. 1530–1532, 2001.

[5] M. Sato, "A new bistatic GPR system using a passive optical sensor for land mine detection", Proceedings of the 2nd International Workshop on Advanced Ground Penetrating Radar, Vol. 1, pp. 164–167, 2003.

[6] R. Tanaka, M. Sato, "A GPR system using a broadband passive optical sensor for land mine detection", Proceedings of the 10th International Conference on Ground Penetrating Radar, Vol. 1, pp. 171–174, 2004.

[7] S.J. Cho, R. Tanaka, M. Sato, "Bistatic GPR by using an optical electric field sensor", Proceedings of the IEEE International Geoscience and Remote Sensing Symposium, Vol. 1, pp. 348–351, 2005.

[8] M. Sato, K. Yoshida, "Bistatic UWB radar system", IEEE International Conference on Ultra-Wideband, Vol. 1, pp. 62–65, 2007.

[9] N. Hayashi, M. Sato, "A fundamental study of bistatic UWB radar for detection of buried objects", IEEE International Conference on Ultra-Wideband, Vol. 2, pp. 125–128, 2008.

[10] T. Takayama, M. Sato, "Evaluation of an array type directional borehole radar system", Proceedings of the IEEE International Geoscience and Remote Sensing Symposium, Vol. 1, pp. 352–355, 2005.

[11] T. Takayama, M. Sato, "A novel direction-finding algorithm for directional borehole radar", IEEE Transactions on Geoscience and Remote Sensing, Vol. 45, pp. 2520–2528, 2007.

[12] T. Takayama, J.H. Kim, M. Sato, "Analysis of directional borehole radar measurement data", Proceedings of the 4th International Workshop on Advanced Ground Penetrating Radar, Vol. 1, pp. 32–35, 2007.

[13] M. Sato, T. Takayama, "A novel directional borehole radar system using optical electric field sensors", IEEE Transactions on Geoscience and Remote Sensing, Vol. 45, pp. 2529–2535, 2007.

[14] M. Sato, T. Takayama, "High range resolution directional borehole radar for 3D fracture delineation", Proceedings of the IEEE International Geoscience and Remote Sensing Symposium, Vol. 1, pp. 132–135, 2009.

[15] H. Gonca Bulur, A. Behzat Şahin, "Fiber optik sensör içeren radar ile gömülü silindirik cisim tespiti", 13. Ulusal Optik, Elektro-Optik ve Fotonik Çalıştayı, 2011.

[16] R. Heinzelmann, A. Stohr, D. Kalinowski, D. Jager, "Miniaturized fiber coupled RF E-field sensor with high sensitivity", 13th IEEE Lasers and Electro-Optics Society Annual Meeting, p. 525–526, Vol. 2, 2000.

[17] P. Neveux, A. Chambarel, "Debye modelisation for the soil moisture measurement in TDR", Proceedings of the IEEE Instrumentation and Measurement Technology Conference, Vol. 1, pp. 187–190, 2006.

[18] C. Leuschen, "Analysis of the complex permittivity and permeability of a Martian soil simulant from 10 MHz to 1 GHz", Proceedings of the IEEE International Geoscience and Remote Sensing Symposium, Vol. 4, pp. 2264–2266, 1999.

[19] Q.A. Naqvi, A.A. Rizvi, Z. Yaqoob, "Scattering of electromagnetic waves from a deeply buried circular cylinder", Progress in Electromagnetics Research, Vol. 27, pp. 37–59, 2000.